Superlattices and Microstructures 69 (2014) 239–252

Contents lists available at ScienceDirect

Superlattices and Microstructures

journal homepage: www.elsevier.com/locate/superlattices

Hydrothermal synthesis, characterizations and photoluminescence study of single crystalline hexagonal ZnO nanorods with three dimensional flowerlike microstructures

Rohidas B. Kale [a,*], Yung-Jung Hsu [b], Yi-Feng Lin [c], Shih-Yuan Lu [d,*]

[a] Department of Physics, Institute of Science, Mumbai 400032, MS, India
[b] Department of Materials Science and Engineering, National Chiao Tung University, Hsinchu 30010, Taiwan, ROC
[c] Department of Chemical Engineering and Materials Program, Chung Yuan Christian University, 200 Chung Pei Rd., Chung Li City 32023, Taiwan, ROC
[d] Department of Chemical Engineering, National Tsing-Hua University, Hsin-Chu 30013, Taiwan, ROC

ARTICLE INFO

Article history:
Received 21 February 2014
Received in revised form 24 February 2014
Accepted 3 March 2014
Available online 12 March 2014

Keywords:
Hydrothermal method
Metal oxide
X-ray diffraction
Scanning electron microscope
Optical properties

ABSTRACT

A simple, low-cost, and environmentally benign hydrothermal approach has been successfully developed to synthesize uniform, large-scale well-crystallized ZnO nanorods with different aspect ratios that were united together to form three dimensional (3D) flowerlike structures. The method involved direct growth of ZnO 3D microstructures using aqueous solution of $Zn(CH_3COO)_2$ as the precursor and NaOH to adjust the pH of resultant solution. Surfactants or templates were not used during the entire synthetic process. Moreover, the morphology evolution of the ZnO nanorods with reaction time suggests a recrystallization–dissolution–growth mechanism that continuously takes place for prolonged interval of time. The XRD pattern of the as-grown ZnO nanorods and relevant analyses confirm the well crystallized hexagonal structure of the ZnO microstructures and no evidence of any other impurity phases. SEM observations reveal that the ZnO product grew in the form of nanorods that were united together to form 3D flowerlike morphology. The high resolution transmission electron microscopy (HRTEM) and selected area electron diffraction (SAED) shows that the ZnO nanorods were single crystalline and grew along the *c*-axis of the crystal plane. PL measurements of the as-synthesized nanorods exhibit excellent excitation features and strong band-edge UV

* Corresponding authors. Tel.: +886 3 571464; fax: +886 3 5715408.
E-mail addresses: rb_kale@yahoo.co.in (R.B. Kale), sylu@mx.nthu.edu.tw (S.-Y. Lu).

http://dx.doi.org/10.1016/j.spmi.2014.03.003

luminescence even at room temperature. The uniform single crystalline, defect free, and high aspect ratio nanorods may find promising applications in optoelectronics and photo-catalysts. The growth habit of ZnO crystal is also illustrated. This method is suitable for large-scale production of ZnO microstructures and could be extended for syntheses of other metal oxides.

1. Introduction

During the past decade, nanomaterials have drawn considerable research attentions, due to their shape and size dependent structural and optoelectronic properties that differ from their bulk counterparts [1–3]. In the present era, numerous researchers are actively engaged not only in syntheses but also to control shape and size of nanostructures that includes nanowires, nanotubes, nanodiscs, nanonails, nanobelts, nanocubes, nanoribbons, nanocables, nanorods, nanospheres and porous nanoscale materials [4–10]. The smallest dimensional structures efficiently transport electrical carriers and may find great applications in many areas, such as electronic, optoelectronic devices, and high performance photo-catalysts [10]. Also, shape and size of nanomaterial greatly affect the physicochemical properties that may be drastically different from those of their bulk counterparts [11]. Researchers have also demonstrated the correlation between the properties of nanomaterial and their morphologies. As an example, ZnO nanorods exhibit improved near band edge emissions than porous nanospheres [12]. The shape of Pt nanoparticles shows noticeable effects on the selectivity of benzene hydengenation [13]. SnO_2 nanospheres with mesoporous structures have better electrochemical performances than the commercially available SnO_2 samples [14]. It was observed that 2D nanowalls of ZnO have a higher transparency than 1D nanospike [15]. Among these numerous morphologies, controlled preparation of three-dimensional (3D) nanostructures composed of one dimensional nanoscale building blocks, has stimulated extensive research attentions due to their enhanced physicochemical properties and superior device performances [16–20]. These hierarchical architectures combine the features of nanoscale building units and can exhibit unique properties that are distinct from those of the low-dimensional structures. As stimulated by both the unique properties and promising applications of such hierarchical architectures, great efforts have been focused on the design of rational methods to organize the nanoscale building blocks into complicated 3D microstructures.

Apart from numerous semiconductors, due to low-cost, environmental friendliness, easy to grow and novel physicochemical properties. ZnO is exhaustively studied and gaining popularity as an intriguing candidate to be used for electronic and photonic devices [21]. It has a direct wide band gap (3.37 eV) with a large exciton binding energy (60 meV), which can ensure sufficient exciton at room temperature with an n-type conductivity and piezoelectric properties [22–25]. These promising properties make it an intriguing candidate to be used in various applications, such as dye sensitized solar cells, UV photon detectors, UV laser diodes, light emitting diodes, field emission displays, gas sensors, active compounds in sunscreens, photo-catalysts, self-cleaning materials, energy harvesting devices (nanogenerators), electronic devices (transistors), piezoelectric transducers, and actuators [26–34].

Previous studies also demonstrated that the properties of ZnO are closely related to the size and shape of the structures. For example, tetrapod ZnO nanostructures exhibit strong UV emissions [35] and needle-like ZnO arrays exhibit strong blue light emissions [36]. Thus, studying the morphology of micro-nanostructure ZnO is an important research topic. As we know, the synthetic method and experimental conditions greatly influence the morphology and/or shape as well as size of a nanomaterial. Therefore, innovative synthetic methods or routes need to be developed for the control over morphology, shape, and size. The most common method to synthesize one-dimensional ZnO nano-/microstructures is the vapor-phase transport process in the presence of metal catalysts,

microemulsion, thermal evaporation of Zn metal, and template-assisted growth [37–40]. However, the introduction of templates to the reaction system makes the process more complicated and as a result impurity may be introduced in the final product. Moreover, the ZnO nanorods grown by the VLS process are usually interlinked together and form bundles with some junctions and defects that occur at elevated temperatures [41]. The poor dispersion of ZnO nanorods/nanowires synthesized by the VLS process may limit their practical applications [41]. Furthermore, preparation of one-dimensional ZnO macro-/nanostructures via solution growth processes without using templates provides a soft and promising route for the large-scale production of uniform or well-dispersed macro-/nanostructures of materials [42,43]. The ZnO nanorods and nanowires were synthesized earlier using microemulsion mediated hydrothermal processes [44,45]. However, it has disadvantages of ultrasonic pretreatment of the mixed solution and the usage of oil, chelating agents, and organic solvents, etc. which were adsorbed on the surface that affect the optical properties of the obtained ZnO nanorods.

Hydrothermal methods have attracted considerable attentions due to their mild reaction conditions, environmental benignancy, easy dispersion in liquid, pollution free, low cost, simplicity, high reaction rate, eco-friendliness, simplicity, low operating temperatures, large scale production, and easy to control preparative parameters [46]. This method gives better control on the morphology as well as size of the synthesized materials by changing the reaction conditions and the obtained product is of high crystalline in nature.

Previous reports are available on the hydrothermally synthesized 1D ZnO microstructures [47–50]. However, non-uniform shape and size with poly-dispersed morphology were clearly seen. Hence, poly-disparity in morphology is still a challenging task during the growth of macro-/nanostructures using hydrothermal method. In the present study, we report on preparation of uniform flowerlike 3D ZnO microstructures consisted of nanorod bundles with different aspect ratios, with a simple hydrothermal method, in the absence of unnecessary organic or inorganic additives, under mild conditions and low zinc concentrations. Subsequently, the influence of reaction time on the aspect ratio of nanorods was also studied.

2. Experimental procedure

All the reagents were of analytical grade (purchased from Showa Chem. Co., Ltd., Japan) and used without further purification. In a typical synthesis process, an appropriate amount of $Zn(CH_3COO)_2$ was dissolved in 50 ml (0.05 M) of deionized water (Milliq 18.2 MΩ) in a beaker. Then 50 ml (1 M) of aqueous solution of NaOH was added into it under constant stirring to get a clear aqueous solution. The pH of the resultant mixture was greater than 12. Then the resultant solution was transferred into a Teflon-container that was further sealed in a stainless steel autoclave. Finally, the autoclave was kept in a hot air oven and the temperature was maintained at 170 °C for 8, 16 and 24 h. After completion of reaction, the autoclave was naturally cooled to room temperature. Subsequently, the resulting solid product was centrifuged, washed with distilled water and ethanol, finally dried at 80 °C in air and used for further characterizations.

The obtained samples were characterized by using different techniques. The crystallographic structure and other relevant information related to structural determination were analyzed using an X-ray diffractometer (XRD, Mac Science, MXP18) with Cu Kα ($\lambda = 1.5406$ Å) radiation over the range $20° < 2\theta < 75°$. The shape, size, and morphology of ZnO microstructures were characterized by using a scanning electron microscope (SEM) (JEOL, JSM-5600) equipped with an energy dispersive X-ray analyzer (EDXA, Oxford Instruments). A small drop of sample dispersed in ethanol was deposited on a carbon grid and then coated with gold (Au) layer for 30 s using an SEM sputter (SPI-Module Sputter Coating Unit, USA), before taking the SEM images. For TEM characterizations, ethanol dispersed samples were deposited over a copper grid pre-coated with carbon. The transmission electron microscope (TEM) and electronic diffraction (ED) patterns were recorded on a JEOL JSM-2010 transmission electron microscope with an acceleration voltage of 200 kV. High-resolution electron microscope (HRTEM) images were obtained from a JEOL JEM-400EX operated at 400 kV. To study the optical properties, optical absorption spectra were recorded using a UV–Visible spectrophotometer (Hitachi Model-3300, Japan). Room temperature photoluminescence (PL) measurements were carried out using a

Hitachi F-4500 fluorescence spectrophotometer equipped with a xenon lamp (150 W) as the light source and photomultiplier (700 V) tube as a detector.

3. Results and discussions

XRD gives information about the crystalline phase, quality, orientation, composition, lattice parameters, defects, stress, and strain of samples. Fig. 1 shows the XRD pattern of the ZnO microstructure synthesized at 170 °C for 16 h and the standard card of bulk ZnO powders (PDF # 36-1451). All diffraction peaks were indexed to a hexagonal wurtzite phase of ZnO, in agreement with the standard pattern. No characteristic peaks of any impurities were detected in the pattern, which confirms that the obtained products are pure ZnO. The comparison of the observed and the standard diffraction peak intensities does not show any preferred orientations. Also, it can be seen that the diffraction peaks are intensive and narrow that confirms the high crystalline nature of the as-synthesized ZnO microstructures. Fig. 2 shows the XRD patterns of the ZnO microstructures obtained at 8 and 24 h. It clearly reveals that the crystal growth of ZnO was not altered with increasing reaction time. It is also worth mentioning that the XRD peak positions of the 3D ZnO microstructures synthesized for 24 h matches exactly with the standard JCPDS data. Only the peak positions of the sample synthesized at 8 h were slightly shifted towards higher angles. It may be due to the initial nucleation and growth that continuously take place during the hydrothermal treatment.

Fig. 3(a) shows a representative EDAX pattern and the details of the relevant elemental analysis for the ZnO microstructure (Inset shows the microstructure region that was used for the elemental analysis). The pattern shows strong Zn and O peaks without any impurity peaks, confirming the purity of the observed ZnO microstructures. The average atomic percentage of the ZnO product is slightly rich in oxygen for the sample synthesized at 8 h. It may be due to presence of some zinc hydroxide species in the sample that decomposes into ZnO in an extended time interval. The average atomic ratio for Zn and O was found to be 1:1, indicating that the products synthesized at 16 and 24 h, were in good stoichiometric ratio. The peaks observed at 0.27 and 2.2 keV are of carbon (C) and gold (Au) due to the carbon grid and gold sputtering, respectively.

Fig. 4(a and b) shows the SEM images of the ZnO product obtained at 170 °C for 8 h. SEM images clearly revealed that the numerous rods united together to form flowerlike three dimensional (3D)

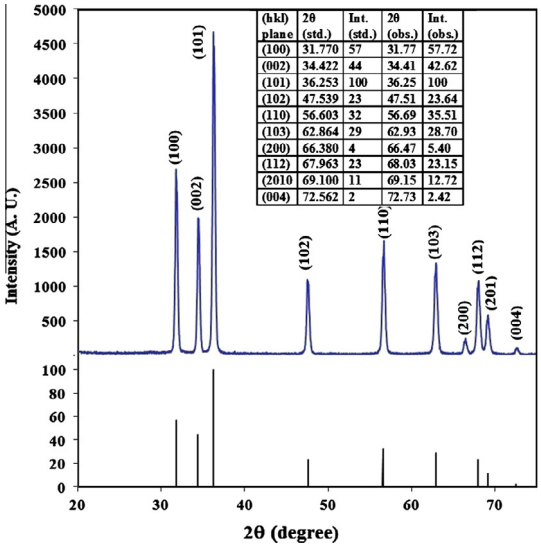

Fig. 1. XRD pattern of ZnO microstructure synthesized with a reaction time of 16 h.

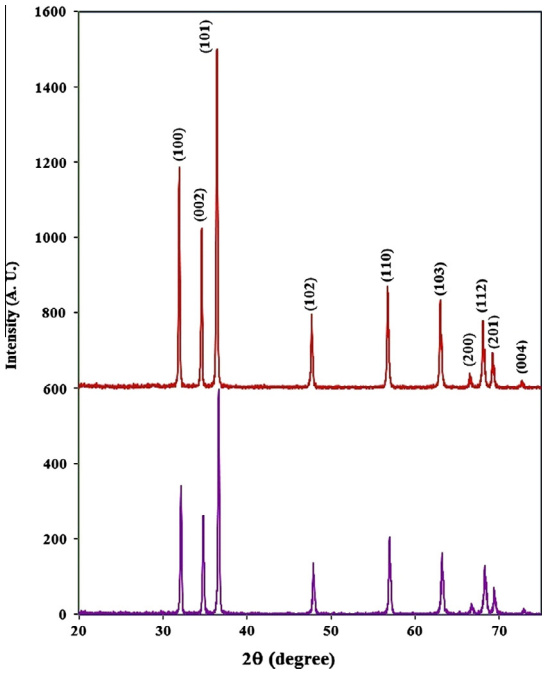

Fig. 2. XRD patterns of ZnO microstructures synthesized with a reaction time of (a) 8 h and (b) 24 h.

structures. The diameter of the nanorods is in the range of 300–500 nm and length is of the order of 6–8 μm. It is worth mentioning that a close observation reveals that some zinc hydroxide species are present at the base of the flowerlike microstructures and also in the surrounding region of the nanorods that are decomposed into ZnO during prolonged time intervals. Also, the core of the microstructures is somewhat bulky that will dissolve in due course of time and diffuse towards outer surfaces of the nanorods. It also reveals that the diameter is slightly thinner at the base of the nanorods and gradually increases (Fig. 4(b)) towards the end. Fig. 5(a and b) shows the SEM images of the ZnO product obtained for a 16 h reaction time. The morphology is more or less the same as that of the product synthesized for a 8 h reaction time. The lower magnification SEM images of ZnO revealed that the flowerlike 3D structures are uniformly distributed over the grid surface and no evidence of polymorphology. Furthermore, it is worth to mention that the diameter of the rod is in the range of 300–400 nm, and the length is increased to 18–20 μm, with high aspect ratio of the order of 50. Such high aspect ratio ZnO nanorods synthesized using a hydrothermal method has been scarcely reported. In addition to this, the diameter of the nanorods slightly but gradually decreases towards the end and the surfaces of the rods are rounded curly. Fig. 6(a and b) shows the SEM images of the ZnO product obtained for a 24 h reaction time. It also reveals flowerlike 3D microstructure consisted of bunches of nanorods with diameter ~1 μm and length 6–8 μm. The SEM image clearly shows pronounced sharp six faced prismatic microrods with flat top faces. Furthermore, the size of the rods tends to be uniform upon the erosion effect of extra base as reported [51]. The rods are bundled together with common crystallographic faces coalescing together due to oriented attachment to lower the surface area and to minimize the surface energy for thermodynamic stability. The oriented attachment mechanism describes the spontaneous self-organization of adjacent particles, so that they share a common crystallographic orientation, followed by the joining of these particles at a planar interface. The decrease in length of the rods can be explained in terms of growth kinetics, by which the fastest growing planes should disappear to leave behind the slowest growing planes as the facets of the product [52]. It is due to the fact that the fastest growing polar surfaces will be dissolved preferentially since this decreases

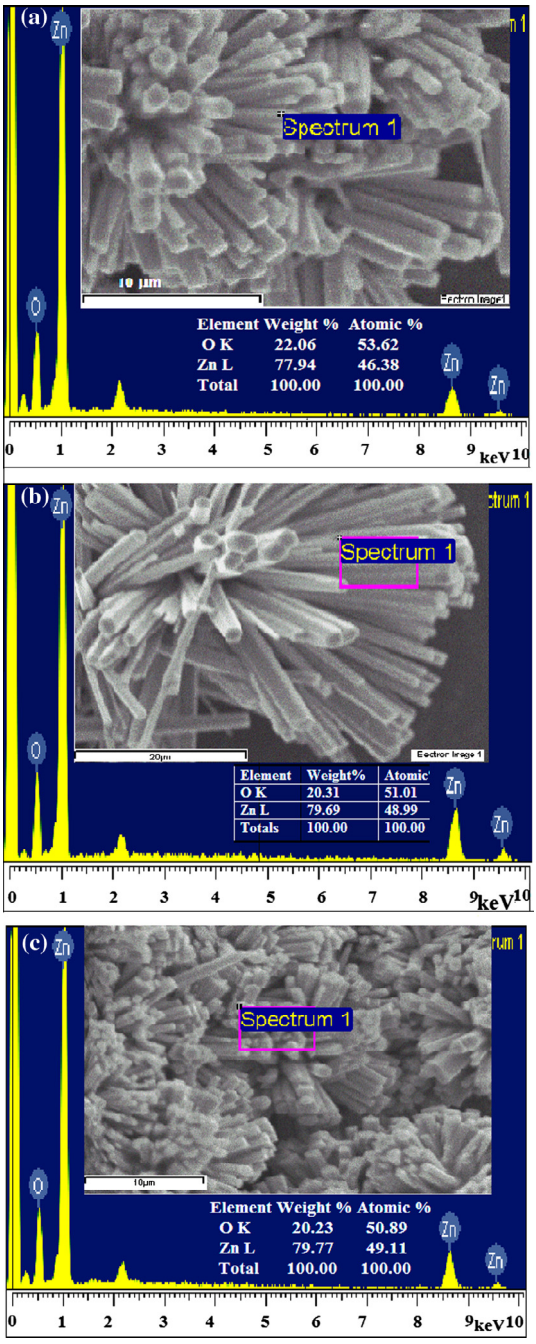

Fig. 3. EDAX pattern of the ZnO microstructures synthesized with reaction time of (a) 8 h (b) 16 h and (c) 24 h (insets shows the elemental analysis and region selected for it).

the system energy during further consequent aging process, and that progressively, leads to the formation of ZnO rods with sharp top surface. Growth morphology is also highly sensitive to the level

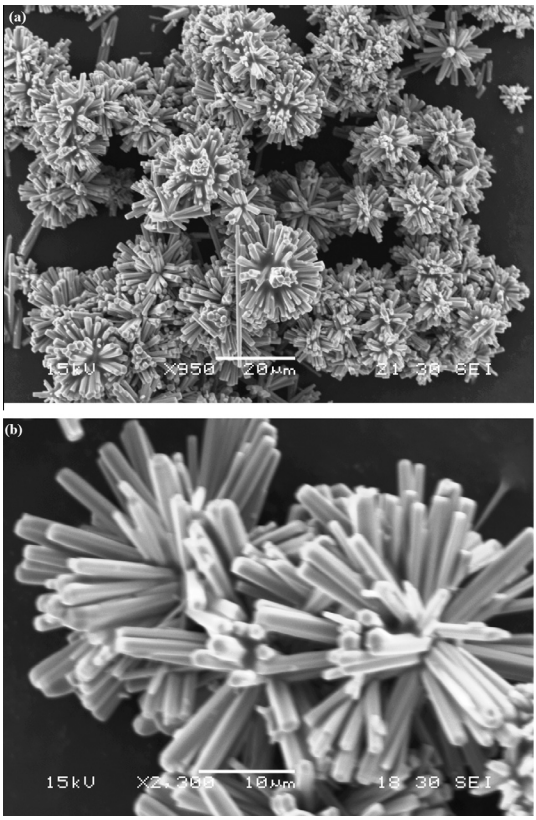

Fig. 4. SEM images of 3D flowerlike ZnO microstructures synthesized with reaction time of 8 h (a) low magnification and (b) high magnification.

of super-saturation. It has been suggested that precipitation should follow the order of sulfate, nitrate, chloride and acetate. Empirical observations followed the order of sulfate, chloride, nitrate, formate and acetate anion. The induction period for baths containing acetate was significantly longer than for baths containing the other salts [53].

In the present hydrothermal conditions, we have synthesized flowerlike ZnO microstructures by the direct decomposition of soluble $Zn(OH)_4^{2-}$ precursor, which follows the growth habit of the ZnO crystals. The crystal growth process involves the following four stages: nucleation, crystal growth, dissolution and recrystallization. Experimental conditions not only affect on the morphology but also on the size of a growing crystal, in which numerous factors integrate to dominate the process. The behavior of crystal growth depends on the aggregation that takes place in the initial induction period and the subsequent growth, diffusion, dissolution, and recrystallization processes. As we know, during the initial reaction period, reaction time affects on the overall size of the aggregation rather than that of the morphology. Subsequent depletion in reactant concentration during a further extension of reaction time, the effects of growth, dissolution and recrystallization processes affect the overall size and morphology.

The formation process of ZnO in aqueous solution is generally suggested through the following reactions:

$$Zn^{2+} + 2(OH)^- \rightarrow Zn(OH)_2 \quad (1)$$

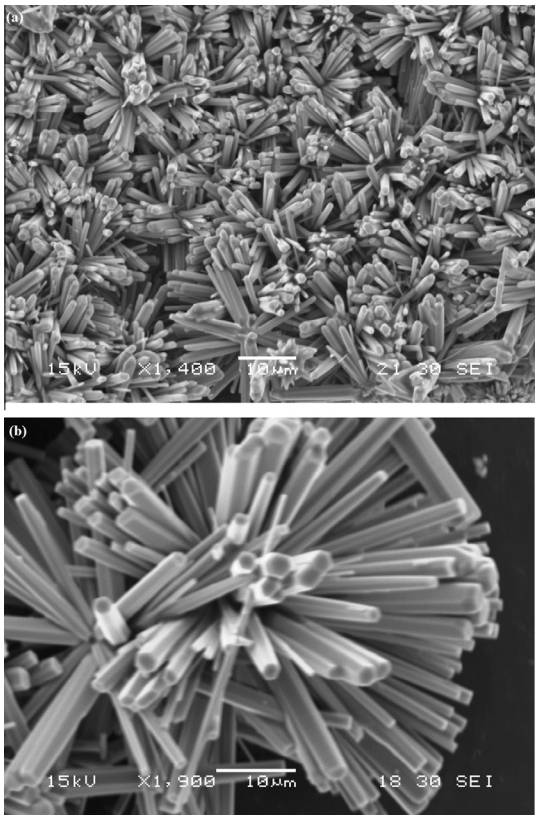

Fig. 5. SEM images of 3D flowerlike ZnO microstructures synthesized with reaction time of 16 h (a) low magnification and (b) high magnification.

$$Zn(OH)_2 + 2OH^- \rightarrow Zn(OH)4^{2-} \quad (2)$$

$$Zn(OH)_4^{2-} \rightarrow ZnO + H_2O + 2OH^- \quad (3)$$

At the initial stage, when limited amount of aqueous alkaline NaOH solution was added, white $Zn(OH)_2$ precipitates were obtained. Further addition of excess sodium hydroxide into the solution however led to the re-dissolution of $Zn(OH)_2$ precipitates to form a homogeneous solution containing $Zn(OH)_4^{2-}$ ions that played a key role in the morphology development of the ZnO crystallites. With the increase in temperature above 160 °C, along with the autogenously generated pressure developed inside the autoclave, the preformed $Zn(OH)_4^{2-}$ ions decomposed to ZnO nanoparticles that acts as seed nuclei. Thus, at the early stage of the reaction, the product was composed of ZnO nuclei that were surrounded by abundant $Zn(OH)_4^{2-}$. At higher concentration of NaOH (1 M) the nucleation followed by crystal growth was relatively fast that resulted in formation of abundant ZnO nanoparticles. Thus at the early stage, ZnO nuclei and growth species of $Zn(OH)_4^{2-}$ coexisted in equilibrium. These preformed ZnO nanoparticles were highly unstable and quickly aggregated into bigger aggregates to minimize the surface energy. In addition, soluble species of $Zn(OH)_4^{2-}$ deposited on the solid surfaces of preformed ZnO nanoparticles. After that, ZnO nanoparticles grew to a stable size, and they continued to grow further by combining with smaller unstable nuclei [54]. Subsequent to this growth, relatively larger particles formed on the surface of the aggregates, smaller and poorly-crystallized nanoparticles were included at the core of the aggregates [55]. Due to the high surface energy of the smaller nano-

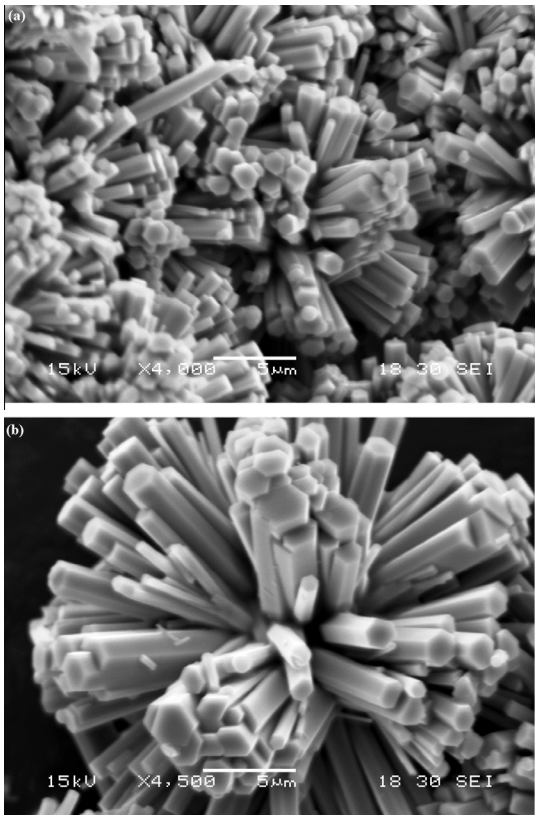

Fig. 6. SEM images of 3D flowerlike ZnO microstructures synthesized with reaction time of 24 h (a) low magnification and (b) high magnification.

particles, that were present in the cores, these smaller nanoparticles can dissolve easily and diffuse outwards. The large nanoparticles located on the surfaces of the bigger aggregates served as the starting growth sites for the subsequent recrystallization process and crystal growth continued [56]. During this process, a rupture of the initial homogeneous nucleation occurred and the growth units were directly incorporated into ZnO crystallites under the present experimental conditions. As the reaction time increased, the concentrations of Zn^{2+} and OH^- gradually decreased and the depletion of these species favored the diffusion, dissolution, and recrystallization processes. These processes dominated only in the latter stage of the morphology evolution during the reforming period, when raw materials became scarce. Thus, during the initial reaction period, the reaction time affects the overall size of the aggregates instead of the morphology. But, when the reactant concentration decreased gradually during the prolonged reaction time period, the effects of diffusion, dissolution, and recrystallization processes affected the overall morphology of the synthesized products. These processes were sensitive to the pH of the reaction mixture, reaction temperature, and autogenously generated pressure [56].

According to the growth habit of ZnO crystals, the relative rates of the ZnO crystal growth in different directions have been $V(0001) > V(01\bar{1}\bar{1}) > V(01\bar{1}0) > V(0000\bar{1})$ reported [57]. Hence, growth units were preferentially supplied for the *c*-axis direction of every nucleus, which caused the generation of numerous randomly distributed ZnO nanorods. Hence, during the diffusion, dissolution, and recrystallization processes, numerous nanorods were grown on the bigger aggregates surfaces due to the preferential attachment of growth units along the *c*-axis, leading to the formation of hierarchical bundle-like architectures. Also, because of the gradual mass diffusion from the inner core to the out-

ermost surface, the rods located on the outer surface grew in length at the expense of the dissolved core materials. Finally, after prolonging the reaction further, the inner cores were consumed completely and the typical flowerlike microstructures assembled with several nanorods were formed [58]. The oriented growth attachment became pronounced after the prolonged time interval. The schematic presentation of the possible growth mechanism of the flowerlike ZnO nanorods is shown in Fig. 7. To support the growth mechanism that is illustrated in Fig. 7, the ZnO product was also synthesized for short reaction periods (4 h) and the SEM image is depicted in Fig. 8. It clearly reveals the aggregation of ZnO nanoparticles, and the numerous bursts originated from the aggregations.

The detailed structural and morphological characterizations of the as-grown ZnO nanorods synthesized for 16 h were also done by TEM and HRTEM equipped with SAED. Fig. 9(a) shows the low-magnification TEM image of the as-grown ZnO nanorods, which is in full agreement with the SEM image in terms of their dimensionality. The SAED pattern of the corresponding nanorod is shown in Fig. 9(b), confirming that the grown nanorods are single crystalline with the wurtzite hexagonal phase and

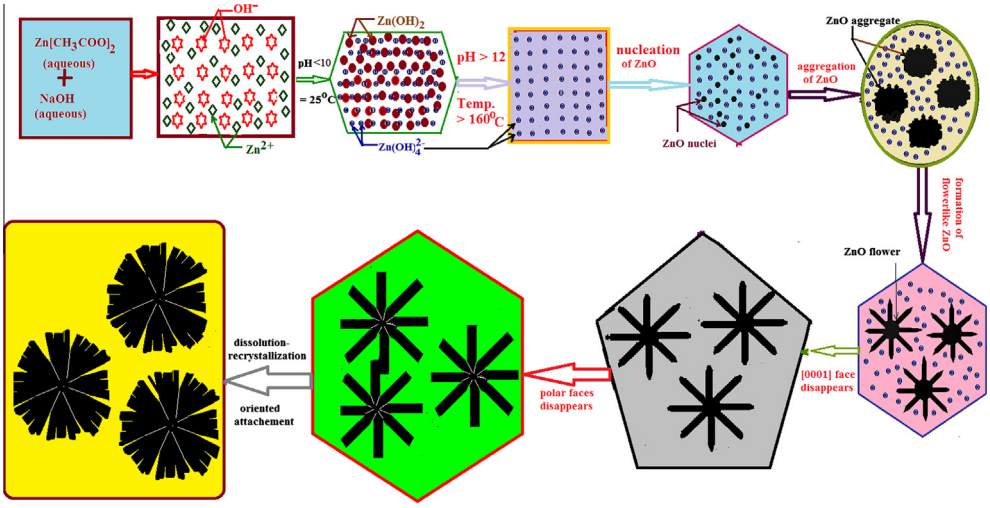

Fig. 7. Schematic representation for the formation of 3D flowerlike ZnO microstructures.

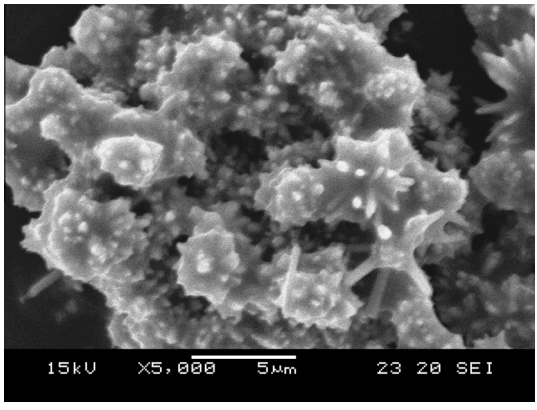

Fig. 8. SEM image of ZnO microstructures synthesized with a reaction time of 4 h.

grown along the (0001) direction. HRTEM image of the nanorod displayed in Fig. 9(a) is shown in Fig. 9(c), which clearly shows well-defined lattice fringes. The distances between two parallel lattice fringes were measured to be about ~0.259 nm, which corresponds to the spacing of the (0001) crystal planes of ZnO with wurtzite hexagonal phase and confirming that the as-grown nanorods are single-crystalline with the wurtzite hexagonal phase and grown along the (0001) direction. The results revealed from the SAED pattern and HRTEM image of the ZnO nanorods are consistent with each other and confirm the single crystalline nature of the nanorods and their growth along the *c*-axis.

It is commonly known that the room-temperature PL spectra for ZnO usually shows four major peaks: a UV emission peak around 380 nm, a blue emission peak around 440–480 nm, a green emission peak around 520 nm, and a red or orange emission peak around 600 nm [59]. The UV peak is attributed to the near band-edge emission, while the other three broad visible bands are generally attributed to the de-excitation process related to defects states in ZnO crystal, such as vacancies and interstitials of zinc and oxygen [60]. Fig. 10 shows the room temperature PL spectra of the ZnO

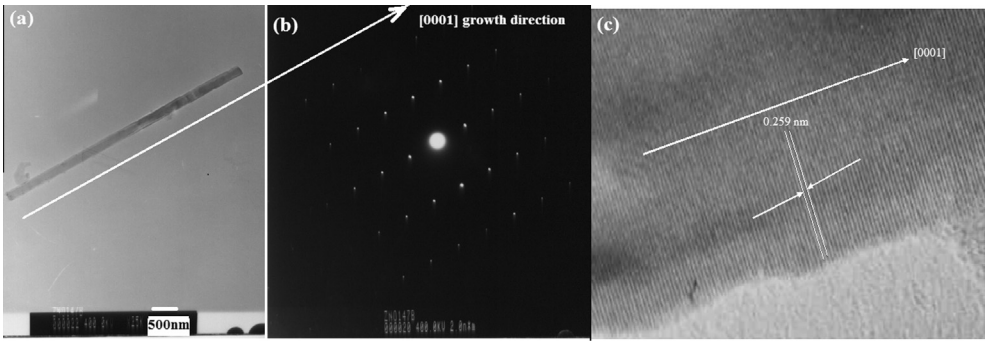

Fig. 9. (a) TEM, (b) SAED and (c) HRTEM image of ZnO nanorod synthesized for 16 h.

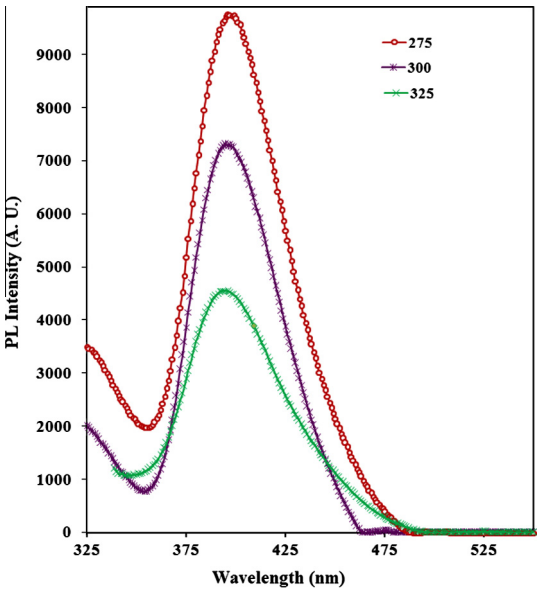

Fig. 10. Room-temperature photoluminescence spectrum of ZnO microstructures synthesized for 16 h.

microstructure under different excitation wavelength. The room temperature PL spectra reveal highly intense peaks centered at 395, 397, and 399 nm (λ_{exc} = 325, 300, and 275 nm)) that correspond to the UV emission. The intense UV emission band is explained by a near band edge transition of the wide band gap ZnO nanorods, namely the recombination of free exciton through an exciton–exciton collision process [61]. The absence of the emission peaks due to impurities and defects in the present synthesized ZnO nanorods indicates excellent optical property free from any defects that are commonly observed for products from hydrothermal syntheses. The PL intensities were found to increase with narrowing FWHM by decreasing the excitation wavelength and the results are in agreement with earlier reports [62]. Previous researchers observed that the PL peaks of ZnO are red-shifted [63,64] with increasing excitation wavelengths. In the present study, no significant red shifts in peaks position were observed with changes in excitation wavelength.

Fig. 11(a and b) shows the SEM images of ZnO microstructures synthesized for 18 h, when the complex reagent NaOH was replaced with NH_4OH, so that the pH of the reaction mixture was ~10, without disturbing other experimental conditions. It clearly reveals the formation of interesting flowerlike 3D structures composed of numerous nanorods with sharp prismatic hexagonal surfaces. It also clearly reveals the existence of polar surfaces with sharp tip of the (0001) plane. The nanorods with sharp and narrow tip are the intriguing candidates for lasing action. It clearly divulges that the complex reagent plays an important role and affects the growth habit of the ZnO nanorods. The schematic representation for growth habit of ZnO crystal under present experimental conditions is shown in Fig. 12.

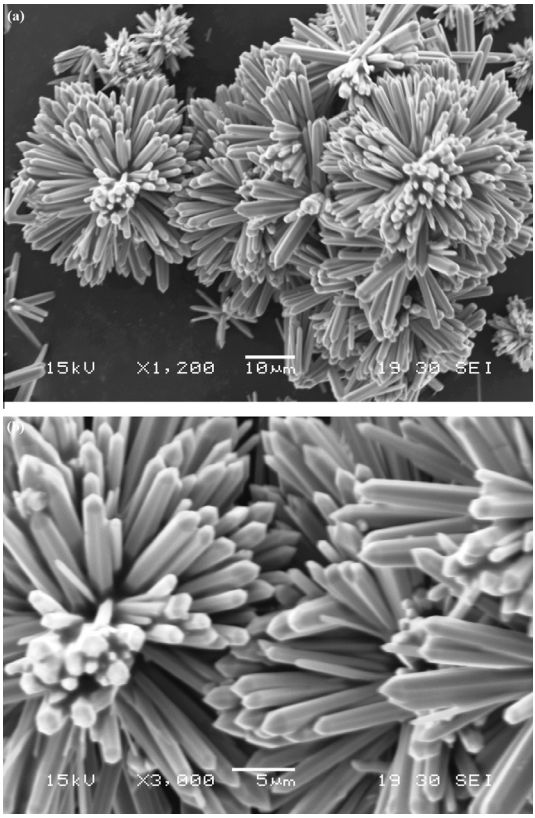

Fig. 11. SEM images of 3D flowerlike ZnO microstructures synthesized for 16 h using NH_4OH (a) low magnification and (b) high magnification.

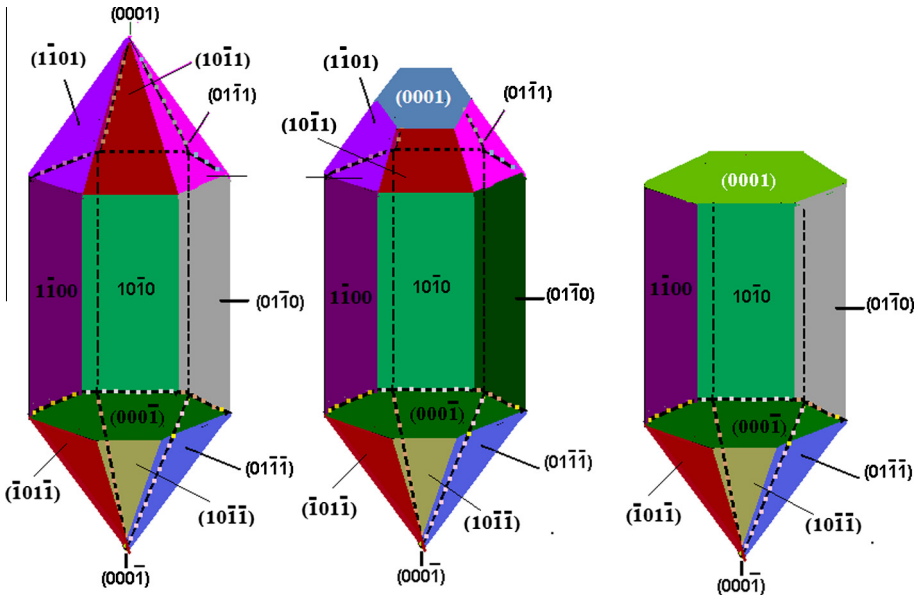

Fig. 12. Schematic representation for growth habits of ZnO crystal under present experimental conditions.

4. Conclusions

In summary, a novel and simple environmentally friendly hydrothermal approach was successfully developed to synthesize single-crystalline ZnO nanorods. The aspect ratio of the nanorods was found to alter with reaction time. The present method does not require complex apparatus and/or sophisticated techniques, or templates. The growth direction of the ZnO nanorods is along the [0001] direction that is consistent with the previous results. A dissolution–recrystallization–decomposition–growth mechanism along with a diffusion process is suggested for the formation of the 3D ZnO flowerlike microstructures. The schematic representation for growth habit of ZnO crystal under present experimental conditions is also depicted. The present method may be utilized to synthesize other metal oxide microstructures. The room temperature PL spectra of as-synthesized ZnO nanorods showed a strong UV emission peak centered at 395 nm. The intensity of the PL emission peak was found to be increased with decreasing excitation wavelength with negligible red-shifts in PL emission peak position. The synthesized ZnO microstructures may have potential applications in optoelectronic devices due to their intense optical emission. The growth habit of the ZnO nanorods not only depends on experimental conditions but also on the initial ingredient present in the reaction mixture.

References

[1] A.P. Alivisatos, J. Phys. Chem. B 271 (1996) 933–937.
[2] R.B. Kale, C.D. Lokhande, J. Phys. Chem. B 109 (2005) 20288–20294.
[3] Y. Zhang, Y. Li, J. Phys. Chem. B 108 (2004) 17805–17811.
[4] Y. Yang, J. Qi, W. Guo, Q. Liao, Y. Zhang, Cryst. Eng. Commun. 12 (2010) 2005–2007.
[5] Z. Liang, X. Cai, S. Tan, P. Yang, L. Zhang, X. Yu, K. Chen, H. Zhu, P. Liu, W. Mai, Phys. Chem. Chem. Phys. 14 (2012) 16111–16114.
[6] R.B. Kale, S.D. Sartale, V. Ganesan, C.D. Lokhande, Y.F. Lin, S.Y. Lu, Appl. Surf. Sci. 253 (2006) 930–936.
[7] V. Suresh, M.S. Huang, M.P. Srinivasan, S. Krishnamoorthy, J. Mater. Chem. 22 (2012) 21871–21872.
[8] X. Huang, L. Shao, G.W. She, M. Wang, S. Chen, X.M. Meng, Cryst. Eng. Commun. 14 (2012) 8330–8334.
[9] Y. Lao, J.Y. Huang, D.Z. Wang, Z.F. Ren, Nano Lett. 2 (2003) 235–238.
[10] (a) Y. Wong, Q. Li, J. Mater. Chem. 14 (2004) 1413–1418;
(b) J.L. Yang, S.J. An, W.I. Park, G.C. Yi, W. Choi, Adv. Mater. 16 (2004) 1661–1664;

(c) Z.R. Tian, J.A. Voigt, J. Liu, B. McKenzie, M.J. McDermott, M.A. Rodriguez, H.K. Xu, Nat. Mater. 2 (2003) 821–826;
(d) G. Wang, D. Chen, H. Zhang, J.Z. Zhang, H.J. Li, J. Phys. Chem. C 112 (2008) 8850–8855.
[11] C.Z. Wen, H.B. Jiang, S.Z. Qiao, H.G. Yang, G.Q. Lu, J. Mater. Chem. 21 (2011) 7052–7061.
[12] G. Yuan, J. Zhu, C. Li, X. Gao, Cryst. Eng. Commun. 14 (2012) 7450–7457.
[13] I. Lee, F. Delbecq, R. Morales, M.A. Albiter, F. Zaera, Nat. Mater. 8 (2009) 132–138.
[14] R.D. Cakan, Y.S. Hu, M. Antonietti, J. Maier, M.M. Titirici, Chem. Mater. 20 (2008) 1227–1229.
[15] D. Pradhan, K.T. Leung, Langmuir 24 (2008) 9707–9716.
[16] H.B. Wu, J.S. Chen, X.W. Lou, H.H. Hng, J. Phys. Chem. C 115 (2011) 24605–24610.
[17] S. Baruah, J. Dutta, Sci. Technol. Adv. Mater. 10 (2009) 013001–0130018.
[18] Z.M. Chen, H. Cao, C.W. Hu, J. Phys. Chem. C 115 (2011) 5522–5529.
[19] Y. Li, Z.J. Si, Y.Q. Lei, X.N. Li, J.K. Tang, S.Y. Song, H.J. Zhang, Cryst. Eng. Commun. 13 (2011) 642–648.
[20] X.L. Cheng, J.S. Jiang, M. Hu, G.Y. Mao, F.X. Bu, C.C. Lin, Y. Zeng, Q.H. Zhang, Cryst. Eng. Commun. 14 (2012) 7701–7708.
[21] D.C. Look, B. Clafin, Y.J. Alivov, S.J. Park, Phys. Status Solidi A 201 (2004) 2203–2212.
[22] J. Bae, J.B. Han, X.M. Zhang, M. Wei, X. Duan, Y. Zhang, Z.L. Wang, J. Phys. Chem. C 113 (2009) 10379–10383.
[23] Y. Sun, G.M. Fuge, N.A. Fox, D.J. Riley, M.N.R. Ashfold, Adv. Mater. 17 (2005) 2477–2481.
[24] Y. Qin, X.D. Wang, Z.L. Wang, Nature 451 (2008) 809–813.
[25] X.D. Wang, J.H. Song, J. Liu, Z.L. Wang, Science 316 (2007) 102–105.
[26] Q. Zhang, C.S. Dandeneau, X. Zhou, G. Cao, Adv. Mater. 21 (2009) 4087–4108.
[27] C.Y. Lu, S.J. Chang, S.P. Chang, C.T. Lee, C.F. Kuo, H.M. Chang, Y.Z. Chiou, C.L. Hsu, I.C. Chen, Appl. Phys. Lett. 89 (2006) 153101–153103.
[28] B.S. Zou, R. Liu, F. Wang, A. Pan, L. Cao, Z.L. Wang, J. Phys. Chem. B 110 (2006) 12865–12873.
[29] S.H. Park, S.H. Kim, S.W. Han, Nanotechnology 18 (2007) 055608.
[30] G. Kenanakis, D. Vernardou, N. Katsarakis, Appl. Catal. A: General 411–412 (2012) 7–14.
[31] V.R. Shinde, T.P. Gujar, C.D. Lokhande, Sens. Actuators B: Chem. 120 (2007) 551–559.
[32] X.D. Bai, E.G. Wang, P.X. Gao, Z.L. Wang, Nano Lett. 3 (2003) 1147–1150.
[33] X.Y. Kong, Z.L. Wang, Nano Lett. 3 (2003) 1625–1631.
[34] A.B. Djuri, X. Chen, Y.H. Leung, A.M. Ching, Ng, J. Mater. Chem. 22 (2012) 6526–6535.
[35] Z.G. Chen, A.Z. Ni, F. Li, H.T. Cong, H.M. Cheng, G.Q. Lu, Chem. Phys. Lett. 434 (2007) 301–395.
[36] T.G. You, J.F. Yan, Z.Y. Zhang, J. Li, J.X. Tian, J.N. Yun, W. Zhao, Mater. Lett. 66 (2012) 246–249.
[37] A. Ishizumi, Y. Kanemitsu, Appl. Phys. Lett. 86 (2005) 253106–253109.
[38] Z.R. Dai, Z.W. Pan, Z.L. Wang, Adv. Funct. Mater. 13 (2003) 9–24.
[39] A. Umar, B.K. Kim, J.J. Kim, Y.B. Hahn, Nanotechnology 18 (2007) 175606.
[40] S.T. Lee, C.H. Liu, J.A. Zapien, Y. Yao, X.M. Meng, C.S. Lee, S.S. Fan, Y. Lifshitz, Adv. Mater. 15 (2003) 838–841.
[41] J. Wang, L. Gao, J. Mater. Chem. 13 (2003) 2551–2554.
[42] X. Wang, Y.D. Li, J. Am. Chem. Soc. 41 (2002) 2446–2461.
[43] T. Kasuga, M. Hiramatsu, A. Hoson, T. Sekino, K. Nihara, Adv. Mater. 11 (1999) 1307–1311.
[44] J. Zhang, L. Sun, H. Pan, C. Liao, C. Yan, New J. Chem. 26 (2002) 33–34.
[45] J.C. Lin, C.P. Lee, K.C. Ho, J. Mater. Chem. 22 (2012) 1270–1273.
[46] H. Wang, J.K. Xiey, Y.M. Duan, J. Mater. Sci. Technol. 27 (2011) 153–158.
[47] R.B. Kale, S.Y. Lu, J. Phys.: Condens. Matter 19 (2007) 096209.
[48] Y. Wang, Z. Hou, H. Guo, L. Shen, G.F. Wang, Q. Zhang, Mater. Lett. 91 (2013) 107–110.
[49] N. Kiomarsipour, R.S. Razavi, Superlattices Nanostruct. 52 (2012) 704–710.
[50] P.K. Giri, S. Bhattacharya, B. Chetia, S. Kumari, D.K. Singh, P.K. Iyer, J. Nanosci. Nanotechnol. 11 (2011) 1–6.
[51] Q.Q.P. Ding, Q.Q. Cao, H.B. Huang, S.G. Yang, X.N. Zhao, Y.W. Du, J. Phys. D: Appl. Phys. 39 (2006) 46–49.
[52] Z.L. Wang, J. Phys. Chem. B 104 (2000) 1153–1175.
[53] K. Govender, D.S. Boyle, P.B. Kenway, P. O'Brien, J. Mater. Chem. 14 (2004) 2575–2591.
[54] H. Colfen, S. Mann, Angew. Chem. Int. Ed. 42 (2003) 2350–2365.
[55] (a) B. Liu, H.C. Zeng, Small 1 (2005) 566–571;
(b) X.X. Yu, J.G. Yu, B. Cheng, B.B. Huang, Chem. Eur. J. 15 (2009) 6731–6739;
(c) W. Cheng, K.B. Tang, Y.X. Qi, J. Sheng, Z.P. Liu, J. Mater. Chem. 20 (2010) 1799–1805.
[56] J. Zhang, L. Sun, J.L. Yin, H. Su, C. Liao, C. Yan, Chem. Mater. 14 (2002) 4172–4177.
[57] A. Smith, R. Rodrıguez-Clemente, Thin Solid Films 345 (1999) 192–196.
[58] X.L. Cheng, J.S. Jiang, M. Hu, G.Y. Mao, F.X. Bu, C.C. Lin, Y. Zeng, Q.H. Zhang, Cryst. Eng. Commun. 14 (2012) 7701–7708.
[59] S.A. Studenikin, N. Golego, M.J. Cocivera, Appl. Phys. 84 (1998) 2287–2294.
[60] (a) X. Liu, X. Wu, H. Cao, R.P.H. Chang, J. Appl. Phys. 95 (2004) 3141–3147;
(b) W.J. Qin, J. Sun, J. Yang, X.W. Du, Mater. Chem. Phys. 130 (2011) 425–430;
(c) R.N. Bhargava, D. Gallagher, X. Hong, A. Nurmikko, Phys. Rev. Lett. 72 (1994) 416–419;
(d) A.G. Joshi, S. Soanl, N. Gandhi, Y.G. Radha Krishna, D. Haranath, Appl. Phys. Lett. 96 (2010) 123102–123104;
(e) W.M. Huang, P. Jiang, C.Y. Wei, D.K. Zhuang, J.L. Shi, J. Mater. Res. 23 (2008) 1946–1952.
[61] Y.C. Kong, D.P. Yu, B. Zhang, W. Fang, S.Q. Feng, Appl. Phys. Lett. 78 (2001) 407–409.
[62] P. Zhang, L.J. Gao, Colloid Interface Sci. 266 (2003) 457–460.
[63] L. Irimpan, B. Krishnan, A. Deepthy, V.P.N. Nampoori, P. Radhakrishnan, J. Phys. D: Appl. Phys. 40 (2007) 5670–5674.
[64] F. Khan, S. Ameen, M. Song, S.H. Shin, J. Lumin. 134 (2013) 160–164.